Petroleum Science 21 (2024) 125–142

Contents lists available at ScienceDirect

Petroleum Science

journal homepage: www.keaipublishing.com/en/journals/petroleum-science

Original Paper

Sedimentary architecture of submarine channel-lobe systems under different seafloor topography: Insights from the Rovuma Basin offshore East Africa

Mei Chen [a, b, c, d], Sheng-He Wu [a, b, *], Rui-Feng Wang [e], Jia-Jia Zhang [a, b], Peng-Fei Xie [f], Min Wang [e], Xiao-Feng Wang [g], Ji-Tao Yu [a, b], Qi-Cong Xiong [a, b]

[a] State Key Laboratory of Petroleum Resources and Prospecting, China University of Petroleum (Beijing), Beijing, 102249, China
[b] College of Geosciences, China University of Petroleum (Beijing), Beijing, 102249, China
[c] Faculty of Geosciences, University of Bremen, Bremen, 28359, Germany
[d] MARUM – Center for Marine and Environmental Sciences, University of Bremen, Bremen, 28359, Germany
[e] Research institute of Petroleum Exploration and Development, PetroChina, Beijing, 10083, China
[f] School of Geosciences, Yangtze University, Wuhan 100083, Hubei, China
[g] CNODC Mozambique Ltd., Beijing 100034, China

ARTICLE INFO

Article history:
Received 16 April 2023
Received in revised form
20 September 2023
Accepted 18 November 2023
Available online 25 November 2023

Edited by Jie Hao and Teng Zhu

Keywords:
Submarine fan
Seafloor topography
Sedimentary architecture
Slope system
SW Indian ocean

ABSTRACT

Seafloor topography plays an important role in the evolution of submarine lobes. However, it is still not so clear how the shape of slope affects the three-dimensional (3-D) architecture of submarine lobes. In this study, we analyze the effect of topography factors on different hierarchical lobe architectures that formed during Pliocene to Quaternary in the Rovuma Basin offshore East Africa. We characterize the shape, size and growth pattern of different hierarchical lobe architectures using 3-D seismic data. We find that the relief of the topographic slope determines the location of preferential deposition of lobe complexes and single lobes. When the topography is irregular and presents topographic lows, lobe complexes first infill these depressions. Single lobes are deposited preferentially at positions with higher longitudinal (i.e. across-slope) slope gradients. As the longitudinal slope becomes higher, the aspect ratio of the single lobes increases. Lateral (i.e. along-slope) topography does not seem to have a strong influence on the shape of single lobe, but it seems to affect the overlap of single lobes. When the lateral slope gradient is relatively high, the single lobes tend to have a larger overlap surface. Furthermore, as the average of lateral slope and longitudinal slope gets greater, the width/thickness ratio of the single lobe is smaller, i.e. sediments tend to accumulate vertically. The results demonstrate that the shape of slopes more comprehensively influences the 3-D architecture of lobes in natural deep-sea systems than previously other lobe deposits and analogue experiments, which helps us better understand the development and evolution of the distal parts of turbidite systems.

1. Introduction

Submarine lobes are typically defined as sand-rich sediments fed by sedimentary gravity flows within submarine channels (Mutti, 1977; Normark, 1978; Lowe, 1982; Mulder and Etienne, 2010; Shanmugam, 2016; Deptuck and Sylvester, 2018; Spychala et al., 2020), and these lobes and channels constitute the channel-lobe systems. Seafloor topography has a significant effect on the characteristics of gravity-driven processes and their related deposits (Kus et al., 2022).

The internal architecture of sediment gravity flow deposits is controlled by the confinement imposed by pre-existing morphology (Lee et al., 1999; Gervais et al., 2006; Prélat et al., 2010; Gamboa and Alves, 2015; Koo et al., 2016; Picot et al., 2016; Chen et al., 2017; Spychala et al., 2017, 2020; Brooks et al., 2018; Kuswandaru et al., 2019; Zhang and Wu, 2019; Fryer et al., 2021; Silva et al., 2020). Confinement is established by a slope that is

* Corresponding author. State Key Laboratory of Petroleum Resources and Prospecting, China University of Petroleum (Beijing), Beijing, 102249, China.
E-mail address: reser@cup.edu.cn (S.-H. Wu).

https://doi.org/10.1016/j.petsci.2023.11.021

steep or slightly oblique to the direction of sediment input (Gervais et al., 2006). Previous studies have indicated that the three-dimensional geometry of lobes is governed by the extent of confinement imposed by the shape and slope of the topography (Gervais et al., 2006; Zhang and Wu, 2019; Spychala et al., 2020). Prélat et al. (2010) conducted a comparative analysis of architectural patterns and quantitative scaling across six significant submarine fan lobe systems, incorporating both outcrop and seismic investigations worldwide. The study found unconfined lobes exhibit attributes of broad distribution and limited vertical extent, whereas confined lobes display relatively constrained distribution and substantial vertical thickness. The two distinct categories of lobe geometries are understood to be associated with differing basin floor topographies. Within confined settings, flows encounter limitations in their ability to disperse, compelling them to build up sediment. Conversely, in less constrained environments, flows possess the capacity to disperse over a wider expanse of the basin, leading to deposits that are more expansive and thinner in nature. Zhang and Wu (2019) employed the well and seismic data to dissect and quantitatively analyze fan lobe deposits within the deepwater region of West Africa. The study differentiated the quantitative configuration disparities between slope lobes and basin lobes. Lobes on the continental slope exhibit limited accommodation space and pronounced lateral constraints. The lobe deposition in basins is significantly impeded by topography, primarily curbing lobe development. Conversely, the environment of the basin floor tends to be more open, characterized by milder lateral limitations and a prevalence of unimpeded lobe expansion. This observed variation in scale primarily stems from the influences of the depositional topography.

Some researchers have conducted quantitative investigations regarding the influence of slope on lobe dimensions through flume experiments (Steel et al., 2017; Spychala et al., 2020). These studies indicate that the length of gravity flow deposits is larger on steep slopes compared to gentle ones (Spychala et al., 2020). Notably, lobes deposited within slope-basin environments tend to be broader than those formed solely on slopes (Steel et al., 2017). In general, the lobes tend to be elongated, narrowed, and thinned as the basin floor angle increases. More pronounced slopes in basin floors enhance sediment transport efficiency, leading to the migration of the depositional center toward the basin (Spychala et al., 2020). The role of topography emerges as a significant factor in the evolutionary processes of lobes.

However, the precise manner in which the slope's configuration influences the three-dimensional (3-D) architecture of submarine lobes within natural deep-marine systems remains somewhat unclear. Presently, research focused on the lobe architecture of natural systems primarily comprises qualitative analyses with limited scope. Additionally, while flume experiments have provided insights into controlling lobe configuration through quantitative gradients, this approach remains somewhat incomplete, often restricted to managing a single lobe via longitudinal gradients. The objective of this study is to examine the impacts of various topographical factors, specifically longitudinal and lateral slopes, on both lobe complexes and individual lobe architecture, encompassing aspects such as shape, size, and stacking patterns.

The study area is located in the Rovuma Basin, offshore East Africa, a zone with channel-lobe systems. This is thus an ideal area for the study of lobe architecture affected by topography factors, especially thanks to the availability of 3-D resolution of seismic data (Chen et al., 2016; Fonnesu et al., 2020; Luan et al., 2021). We aim to use this data to deepen the relationship between the finer parameters contained in the sedimentary topography and control the lobe architecture, which is expected to provide a fine characterization of the lobe architecture in a system, which can guide the study of depositional patterns in similar cases.

2. Setting

2.1. Geological setting

The Rovuma Basin is bounded to north-eastern Mozambique and south-eastern Tanzania (Fig. 1a). Our study area (Fig. 1b) is located in the deep-water area of the Rovuma Basin, at water depths of more than 1500 m. It is located 80 km east of the northern coastline of Mozambique and south of the Rovuma River delta (Fig. 1a and b). The deep-water area of the basin can be divided into three units from west to east, namely the shelf-slope area, the Kerimbas Graben Belt and the Davie uplift belt. Rovuma Basin is in a north-south orientation (Fig. 1b) (Chen et al., 2016; Cao et al., 2018), with a narrow continental shelf (5–30 km) and a steep continental slope (3°–5°, western part). The study area is located between the lower continental slope between the Palma thrust belt in the west and the Kerimbas Graben Belt in the east (Figs. 1c and 2a).

Basins offshore East Africa have evolved over the Mesozoic period, prompted by the rifting of Eastern Gondwana and the formation of the Indian Ocean. The initial onshore uplift in East Africa, coupled with deltaic advancement, gave rise to the development of gravity sliding and salt diapirs within the Rovuma Basin. Subsequently, during the Oligocene to Pliocene period, the East Africa normal fault zone and the East Africa thrust fault zone took shape (as depicted in Fig. 1b and c) (Zhang et al., 2018). Simultaneously, owing to the continued uplift of the East African continent, the Rovuma Delta expanded seaward, resulting in substantial terrigenous clastics deposition on the shelf. These sediments then cascaded along the continental slope and settled into the deep sea, thereby giving rise to a substantial gravity detachment structure. (Chen et al., 2016; section a-a' in Fig. 1b).

The Rovuma Basin is an offshore environment mainly fed by the Rovuma River system. Sediment gravity flows from the Rovuma delta are transported from west to east to the deep-water area (Liu et al., 2017; Luan et al., 2021). From the Miocene to the present, gravity flow deposits such as submarine fans developed in a large area of the deep-sea part of the Rovuma Basin (Chen et al., 2016). The interval of interest of the present study corresponds to Pliocene - Quaternary (Fig. 2a and b) that is located at depths in 2000–3000 m.

2.2. Oceanography setting

Currently, the prevailing oceanic current system within the Rovuma Basin is primarily shaped by the bifurcation of the westward-moving Northeast Madagascar Current. This division gives rise to the East African Coastal Current, which proceeds in a northward direction, while another current flows southward toward the Mozambique Channel (Breitzke et al., 2017; Collins et al., 2016). Bottom currents associated with intermediate water masses, such as the Antarctic Intermediate Water (AAIW) as depicted in Fig. 1a, and deep-water masses including the North Atlantic Deep Water (NADW) and Antarctic Bottom Water (AABW), predominantly travel northward along the northern Mozambican margin (Fig. 1b; Collins et al., 2016; Fuhrmann et al., 2020; Miramontes et al., 2021; Chen et al., 2023).

3. Material and methods

3.1. Material

Available seismic data are used in our study. They were imported and analyzed in Geoscope software. The vertical axis has

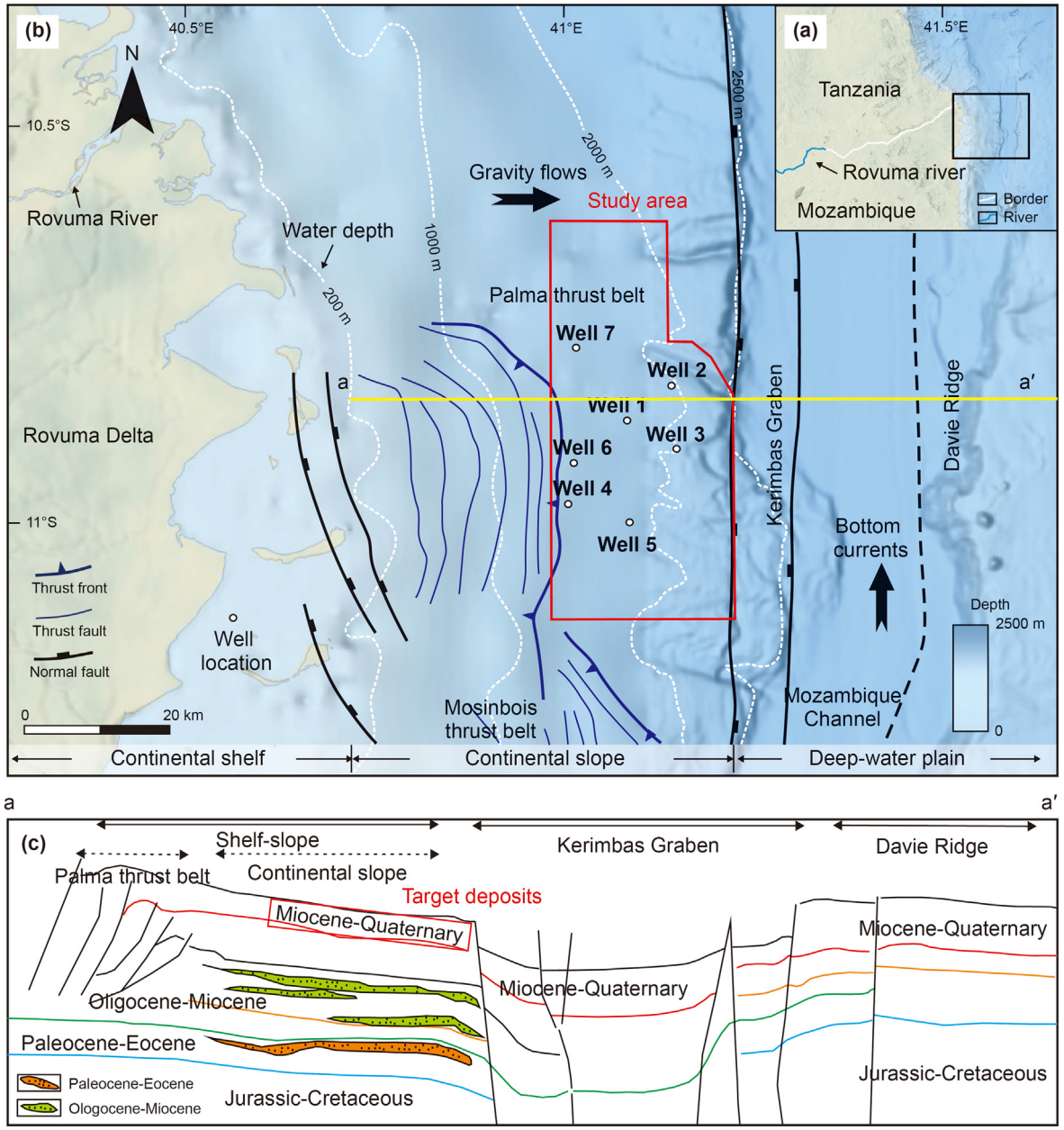

Fig. 1. (a) Geographic location map of the study area (black frame). (b) Bathymetric and topographic map showing the location of the study area (red frame, same range as seismic data), and the main tectonic and sedimentary features. (c) Sectional structural location map of the study area (the position corresponds to the yellow line in Fig. 1b, according to Zhang et al. (2018).

been converted to depth. Seismic data cover the entire extent of the study area. The vertical resolution in interval of interest is approximately 12.5 m. It is negative polarity of the Society of Exploration Geophysicists (SEG). Seven well data were processed using Direct software, which integrates well information. The resolution of the data sets (well and seismic data) used in the present study allows us to analyze lobe complexes and single lobes.

3.2. Seismic interpretation and sedimentary architecture identification

Wide and continuous high-amplitude seismic reflections could be identified as sequences' and architectures' boundaries thanks to the combination of well and seismic data (Vail, 1987). Sequences and channel-lobe systems are recognized and classified from seismic data. The Pliocene-Quaternary strata are divided into five sequences: sequence 1 (Sq1), sequence 2(Sq2), sequence 3(Sq3), sequence 4(Sq4) and sequence 5(Sq5) (Fig. 4). Within the sequences, based on the sandstone assemblage in wells, as well as the geometry, extent and boundaries of seismic units, the different hierarchical architectures can be identified.

We adopted the general lobe architecture hierarchy partitioning scheme, i.e. lobe complexes, single lobes and lobe elements (Mutti and Normark, 1987; Deptuck et al., 2008; Prélat et al., 2010; Straub and Pyles, 2012; Picot et al., 2016; Zhang and Wu, 2019). A single lobe presents a complete lobe shape in plan view and a complete bottom-flat top-convex shape in cross-section (Picot et al., 2016; Zhang and Wu, 2019). The amplitude of the main body of the lobe is higher than that of the lobe margin. A lobe complex can be identified as a combination of several single lobes. Submarine channels

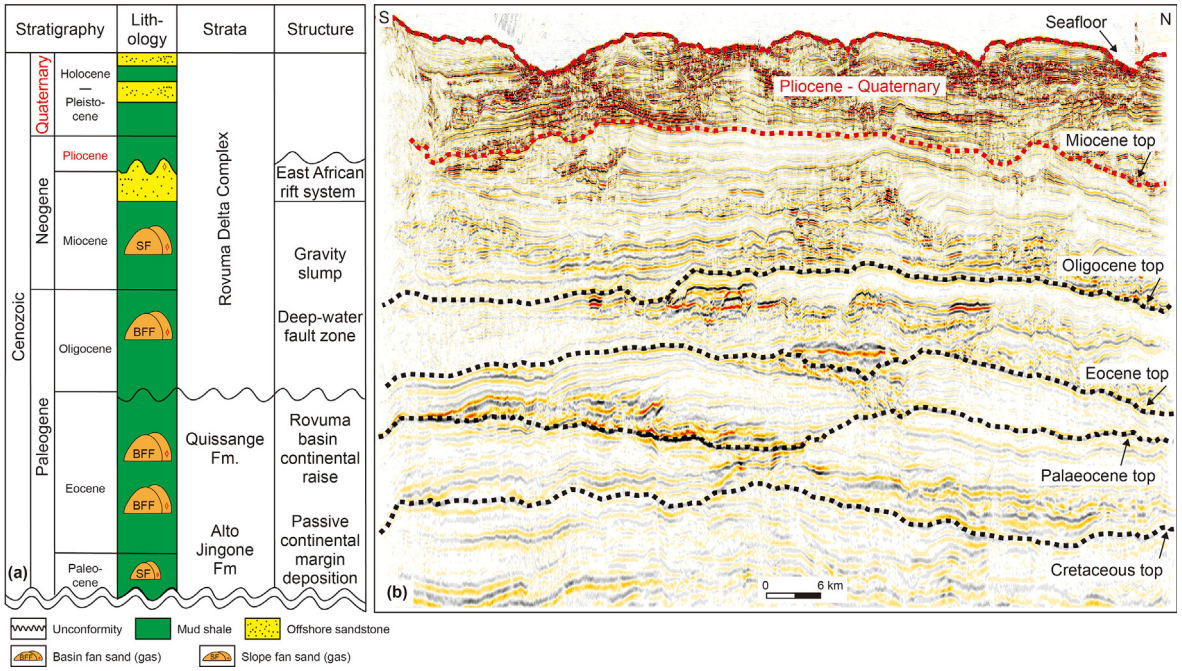

Fig. 2. (a) Stratigraphy of the study area (modified from Zhang et al., 2018). The target formation of this study is the Pliocene – Quaternary strata. (b) Section a-a' map of the study area (the position corresponds to the yellow line in Fig. 1a).

presents a U-shaped shape in section and can be either symmetric or asymmetric. The floor of submarine channels is typically coarser than the levees and the surrounding (hemi) pelagic deposits, and they can thus be identified in seismic data as elongated areas in plan view of high amplitude reflections (Deptuck and Sylvester, 2018). Fig. 3 shows the example of the method used for the identification of lobe and channel features in seismic plane (Fig. 3a) and profile (Fig. 3b).

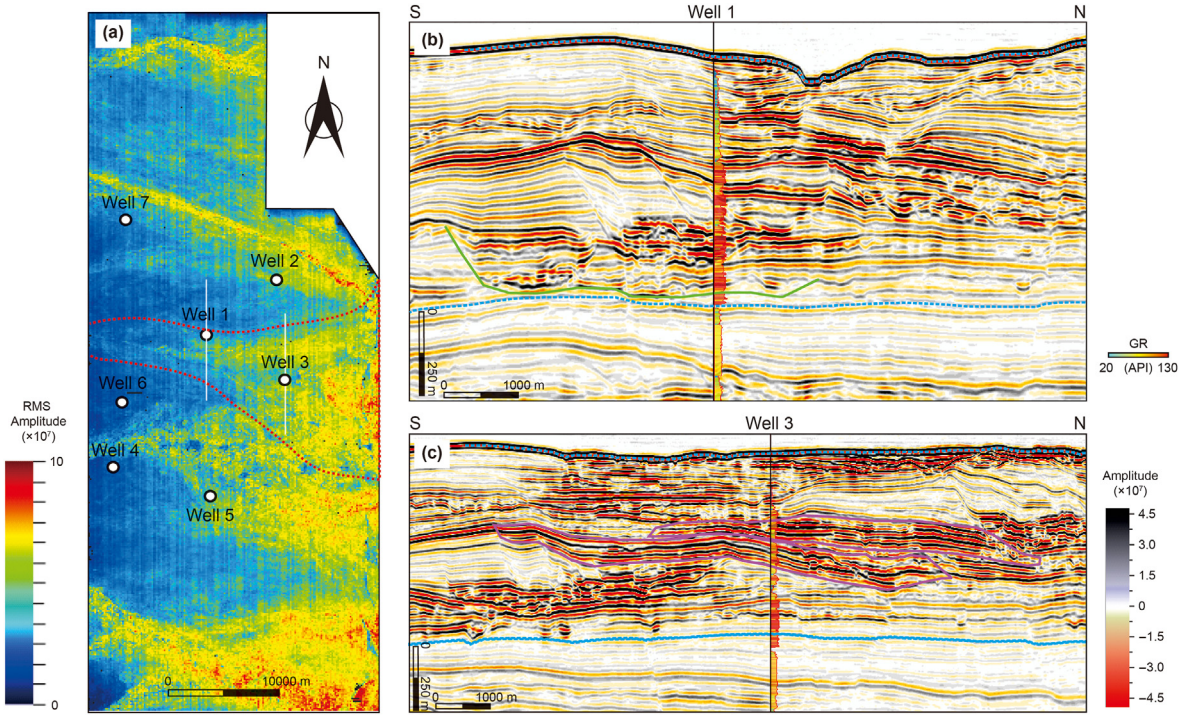

Fig. 3. Example of the method used for the identification of lobe and channel features in root mean square (RMS) map (a) and seismic profiles (b) and (c). (a) Lobe and channel features (red dashed lines) identified using the RMS amplitude extraction of the Pliocene-Quaternary deposits located between Pliocene and Quaternary strata (cyan dashed lines) in Fig. 2b and the seafloor. (b) Channel features (green solid line) identified on a seismic profile correlated with gamma ray measurements on Well 1. (c) Lobe features (rose pink solid lines) identified on a seismic profile correlated with gamma ray measurements on Well 3. The boundary of the seismic reflection is the boundary of the lobes.

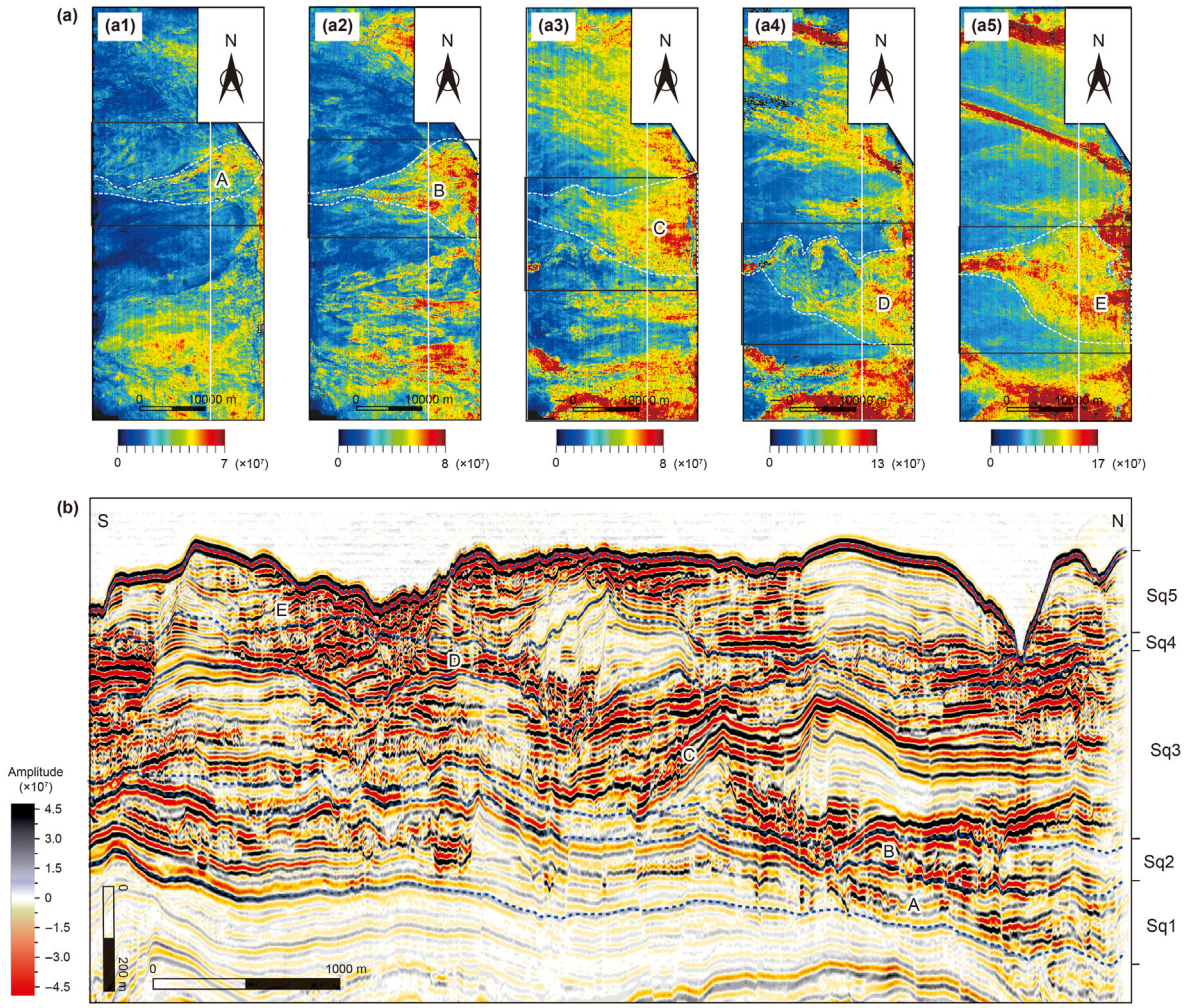

Fig. 4. (a) RMS amplitude maps of Pliocene-Quaternary deposits (architectural complexes A, B, C, D and F). The white lines represent the location of the seismic profile shown in (b). (b) Seismic reflection profile showing the different architecture complexes bounded by blue dashed lines.

3.3. Acquisition of topography parameters

Elevation maps and slope maps of the topography before lobe architectures were made in PaleoScan software. Elevation maps display the variation in height and elevation. We mapped the elevation data obtained by tracking the horizon. Longitudinal slope (i.e. across-slope) was calculated in the west-east direction of dip degree. First, we set up a main line along the submarine channel and the lobe. Then, we calculated the average value of the main line as longitudinal slope dip degree (°). For lateral slope (i.e. along-slope), we calculated the average value of vertical mainline (north-south direction).

4. Results

4.1. Hierarchies of the lobe architecture

Channel and lobe architectures are recognized and classified from seismic data following the criteria explained in Section 3.2. The Pliocene-Quaternary strata are divided into five sequences: Sq1, Sq2, Sq3, Sq4 and Sq5 (Fig. 4). Within the sequences, the different hierarchical architectures are identified, including architectural complexes (A, B, C, D and E; Fig. 4), architectural elements (A1 and A2, B1 and B2, C1 and C2, D1 and D2, E1 and E2; Fig. 5).

4.1.1. Lobe complexes

Architectural complexes can be divided according to high-amplitude regions. The assemblies of strip-shaped and lobe-shaped reflection can be recognized as an architectural complex system.

In the root mean square (RMS) amplitude maps, architectural complexes differ in deposition location and morphology. Architectural complexes A-E all show banded shape in the west (Fig. 4a). These strip-shaped zones present different widths and curvatures. They gradually fan out in the middle and appear as lobe shape in the east (Fig. 4a). Their lobe-shaped zones are lenticular-shaped areas with high amplitude and show variable thickness in the seismic reflection profiles (Fig. 4b). From architectutal complexes A to E, the area of high amplitude values migrates southward (Fig. 4a and b).

4.1.2. Single lobes

A single lobe stands as the fundamental genetic unit within the context of a single feeder channel. Typically, it exhibits a fully formed lobe shape. Vertically, it comprises lobe elements that share similar rhythms across multiple intervals, along with incremental variations in the degree of sandstone intercalation (Zhang and Wu, 2019). Architectural complexes A-E are all susceptible to division into two distinct individual architectural components. It is

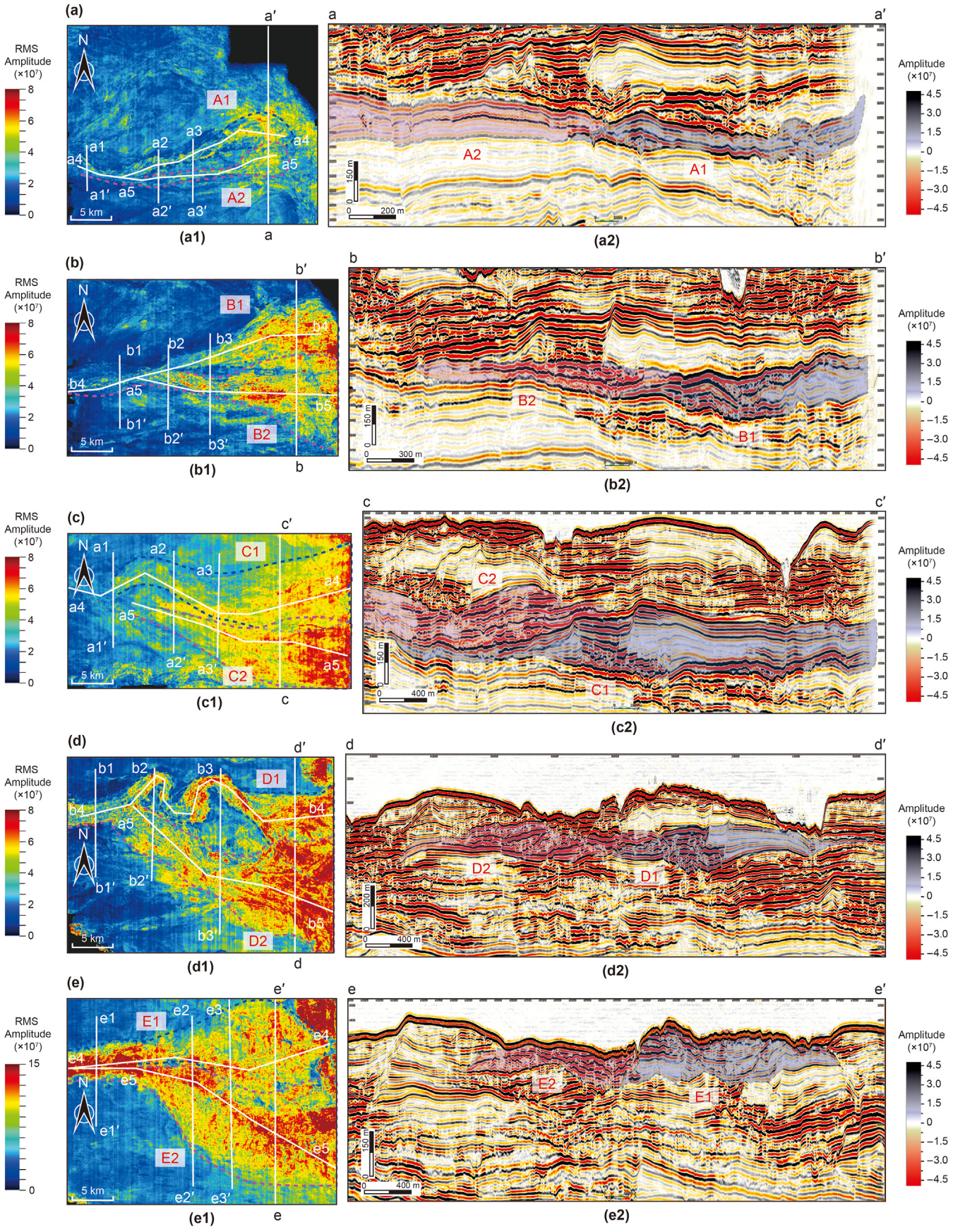
(a)
a′
a
a′
RMS Amplitude (×10⁷)
8
6
4
2
0
N
A1
a1
a2
a3
a4
a5
a1′
a2′
a3′
A2
5 km
(a1)
a
A2
A1
150 m
0
200 m
(a2)
Amplitude (×10⁷)
4.5
3.0
1.5
0
−1.5
−3.0
−4.5
(b)
b′
b
b′
B1
b1
b2
b3
b4
a5
b5
b1′
b2′
b3′
B2
5 km
(b1)
B2
B1
300 m
(b2)
(c)
c′
c
c′
C1
C2
a1
a2
a3
a4
a5
a1′
a2′
a3′
5 km
(c1)
400 m
(c2)
(d)
d′
d
d′
D1
D2
b1
b2
b3
b4
a5
b1′
b2′
b3′
b5
5 km
(d1)
400 m
(d2)
(e)
e′
e
e′
RMS Amplitude (×10⁷)
15
0
E1
E2
e1
e2
e3
e4
e5
e1′
e2′
e3′
5 km
(e1)
400 m
(e2)

noteworthy that the single lobes within diverse lobe complexes showcase considerable disparities, while maintaining a certain degree of similarity within a given complex.

1) Architectural complex A contains two small-scale architectural elements with crescent-shaped areas of high amplitude reflections that form the main body of a single lobe. Low-amplitude regions surround the lobe body with a small radius (1–3 m) (Fig. 5a). On profile view, architectural elements show sheet-shaped zones with high amplitude in the middle and weak amplitude on both sides (Fig. 5(a2)). The right margin of single element A1 diverges from the left margin of single element A2 (Fig. 5(a2)).

2) The amplitude of north architectural element B1 is higher and stronger than southern architectural element B2 (Fig. 5(b1)). The RMS amplitude map shows that elements B1 and B2 are tongue-shaped and larger than architectural elements A1 and A2. On the profile, for architectural elementB1, the amplitude in northern side is obviously stronger than that on the southern side. The right margin of single element B1 diverges from the left margin of single element B2 (Fig. 5(b2)).

3) The area of the western strip-shaped amplitude in architectural complex C is wider than architectural complexes A and B, spreading out to the east (Fig. 5(c1)). The RMS amplitude map shows a fan-shape of high amplitude. The right margin of single element C1 diverges from the left margin of single element C2 (Fig. 5(c2)), whose overlapping area is larger than architectural complexes A and B.

4) The area shape of northern strip-shaped amplitude in architectural complex D is curved (Fig. 5(d1)). The two architectural elements are scattered further east (Fig. 5(d1)). The right margin of single element D1 diverges from the left margin of single element D2 (Fig. 5(d2)).

5) The plane intersection area in the two single elements of architectural complex E is relatively close (Fig. 5(e1)). In the profile map, the right margin of single element E1 diverges from the left margin of single element E2, and the two architectural elements slightly overlap (approximately 300 m) (Fig. 5(e2)).

According to the above observation, architectural complexes A-E are interpreted as channel-lobe complexes. Architectural elements A1 and A2, B1 and B2, C1 and C2, E1 and E2 are interpreted as single channel-lobes (Fig. 6). The single lobes within lobe complexes (A, B, C, D and E) were all preferentially deposited in the north, showing southward migration.

4.2. Characteristics of the lobe architectures

Architectures of a lobe include their shape, size and growth characteristics. We analyze lobe complexes' and single lobes' architecture features by using seismic data.

4.2.1. Lobe shape and size

Lobes vary greatly in size and shape, although the maximum extent of some of them could not be identified due to limitation in the data coverage (Fig. 6, Table 1). The smallest mapped lobe is 4578 m in length and 3037 m in width (A1). The largest mapped lobe is 10360 m long by 8061 m wide (D2). Some lobes are very elongated (12548 m long by 6877 m wide, C1), but many are relatively rounded. Lobes generally have a length to width ratio of 2.52 to 1.03 (averaging approximately 1.66). All of the mapped lobes are round or elongated in the dip direction (east to west). Most lobes are irregular ovoids in map view with an average width of 5490 m and an average length of 8602 m. Lobes are commonly lenticular cross section with a maximum thickness of 66–224 m and an average maximum thickness of 127 m (Table 1).

4.2.2. General growth characteristics

4.2.2.1. Lobe A. For architectural complex A, the zones of high amplitude are characterized by U-shapes (Fig. 7(a1), (a2) and (a3)) and sheet-shapes (Fig. 7(a4) and (a5)) on the seismic profiles. The U-shape zones of the seismic reflection becomes smaller and the amplitude increases from west (Fig. 7(a1) and (a2)) to east (Fig. 7(a3)) towards the basin. The zone of the sheet-shapes' seismic reflection gradually becomes stronger and thicker (Fig. 7(a4) and (a5)).

4.2.2.2. Lobe B. For architectural complex B, the zones of high amplitude are characterized by U-shapes (Fig. 7(b1), (b2) and (b3)) and sheet-shapes (Fig. 7(b4) and (b5)) on the seismic profiles. The U-shaped zones are distributed from the main channel at the beginning, initially overlaps, and then gradually separates into two parts. (Fig. 7(b1), (b2) and (b3)). Towards the basin, the zone of the sheet-shaped seismic reflection gradually becomes higher and thicker (Fig. 7(b4) and (b5)).

4.2.2.3. Lobe C. For architectural complex C, the zones of high amplitude are characterized by U-shapes (Fig. 7(c1), (c2) and (c3)) and sheet-shapes (Fig. 7(c4) and (c5)) on the seismic profiles. The U-shaped zones begin to separate and then overlap again (Fig. 7(c1), (c2) and (c3)). Towards the basin, the zone of the sheet-shaped seismic reflection gradually becomes higher and thicker. The thickness of the sheet-like amplitude region is greater than that of lobes A and B (Fig. 7(c3) and (c4)).

4.2.2.4. Lobe D. For architectural complex D, the zones of high amplitude are characterized by U-shapes (Fig. 8(d1), (d2) and (d3)) and sheet-shapes (Fig. 8(d4) and (d5)) on the seismic profiles. The U-shaped zones begin to separate and then cross again (Fig. 8(d1), (d2) and (d3)), meaning that it has a high degree of curvature. Towards the basin, the zone of the sheet-shaped seismic reflection gradually becomes stronger and thicker (Fig. 8(d4) and (d5)). Compared with lobes A, B, C and D, its U-shaped reflection area extends farther.

4.2.2.5. Lobe E. For architectural complex E, the zones of high amplitude are characterized by U-shapes (Fig. 8(e1), (e2) and (e3)) and sheet-shapes (Fig. 8(e4) and (e5)) on the seismic profiles. The U-shaped zones begin to separate and then cross again (Fig. 8(e1), (e2) and (e3)), meaning that it has a high degree of curvature. Towards the basin, the zone of the sheet-shaped seismic reflection gradually becomes stronger and thicker (Fig. 8(e4) and (e5)). Compared with lobes A, B, C, D and E, its turning position where the feeder channel is dispersed into lobes tends to the basin.

Feeder channels vary greatly in size and shape (Fig. 6; Table 2). The smallest channel complex is 107 m thickness by 1152 m width (A). The largest channel complex is 179 m thickness by 2057 m width (C). The smallest single channel is 64 m thickness by 1136 m width (A2). The largest single channel is 163 m thick by 2321 m wide. Single channels are commonly U-shaped in cross section with a maximum thickness of 64–163 m and an average maximum thickness of 107.4 m (Table 2).

Fig. 5. Seismic RMS maps and seismic profiles of depositional architectural complexes A, B, C, D and F. The white lines (a1), (b1), (c1), (d1) and (e1) represent the location of the seismic profiles shown in (a2), (b2), (c2), (d2) and (e2). The blue dashed lines represent the boundaries of the first deposit. The pink dashed lines represent the boundaries of the second deposit. The filled colors represent the architectural complexes A, B, C, D, E and F deposits in (a2), (b2), (c2), (d2) and (e2).

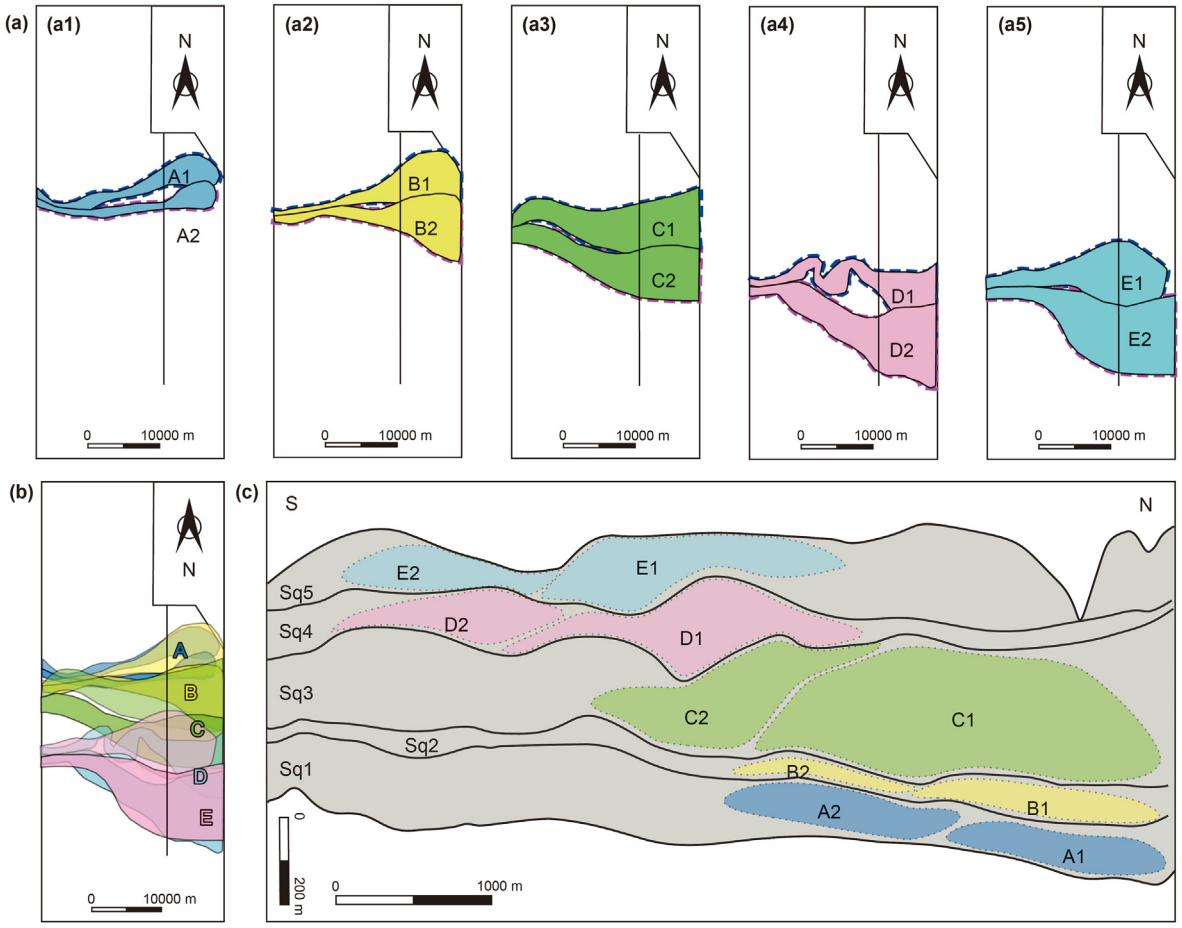

Fig. 6. Interpretation of architectural complexes and architectural elements. (a) Maps showing architectural elements. (b) Map showing all architectural elements. (c) Sectional facies diagrams of architectural elements and architectural complexes. The black lines of (a) and (b) represent the location of the depositional profile of (c).

Table 1
The parameters of different hierarchical lobes, including length, width, length/width, average of length and width and maximum thickness.

Lobe complex	Single lobe	Length, m	Width, m	Length/width	Average of length and width, m	Maximum thickness, m
A	A1	4578	3037	1.51	3807.5	110
	A2	5539	3422	1.62	4480.5	115
B	#B1	[a]10573	6877	1.54	8725.0	99
	#B2	[a]7182	[a]3542	2.03	5362.0	66
C	#C1	[a]12548	[a]4979	2.52	8763.5	224
	#C2	[a]9828	[a]5115	1.92	7471.5	172
D	#D1	[a]>8080	[a]6978	1.16	7529.0	168
	#D2	[a]>10360	[a]8061	1.29	9210.5	81
E	E1	8776	8541	1.03	8658.5	144
	#E2	[a]>8553	[a]4246	2.01	6399.5	90

#Incomplete lobe.
[a] Maximum value in plan view.

4.3. Topography before the lobe architecture deposits

The topography parameters were measured following the method explained in Section 3.3. We analyzed the topographic features before the lobe deposition from two parts: longitudinal slope and lateral slope.

4.3.1. Longitudinal slope

Fig. 9 shows the topographic maps (Fig. 9a) and slope maps (Fig. 9b) before the lobe deposits. It shows the low terrain zone gradually migrates southward. In the downstream part of the lobe, there is a large step, representing a landslide (Fig. 9b). The overall slope dip is large in the west (feeder channel location) and small in the east (Fig. 9b). It reflects that the lobe deposit area is located in a slope system that is high in the west and low in the east.

Table 3 shows the specific parameters of the longitudinal slope. Longitudinal slope varies greatly, ranging from 0.37° to 4.33°. The difference in slope ranges from 0.15° to 1.13°. Average longitudinal slope ranges from 0.73° to 4.26°. The last deposited lobe E has a large longidinal slope, and the average longinal slope of other lobes is similar with a avearge longitudinal slope 0.87.

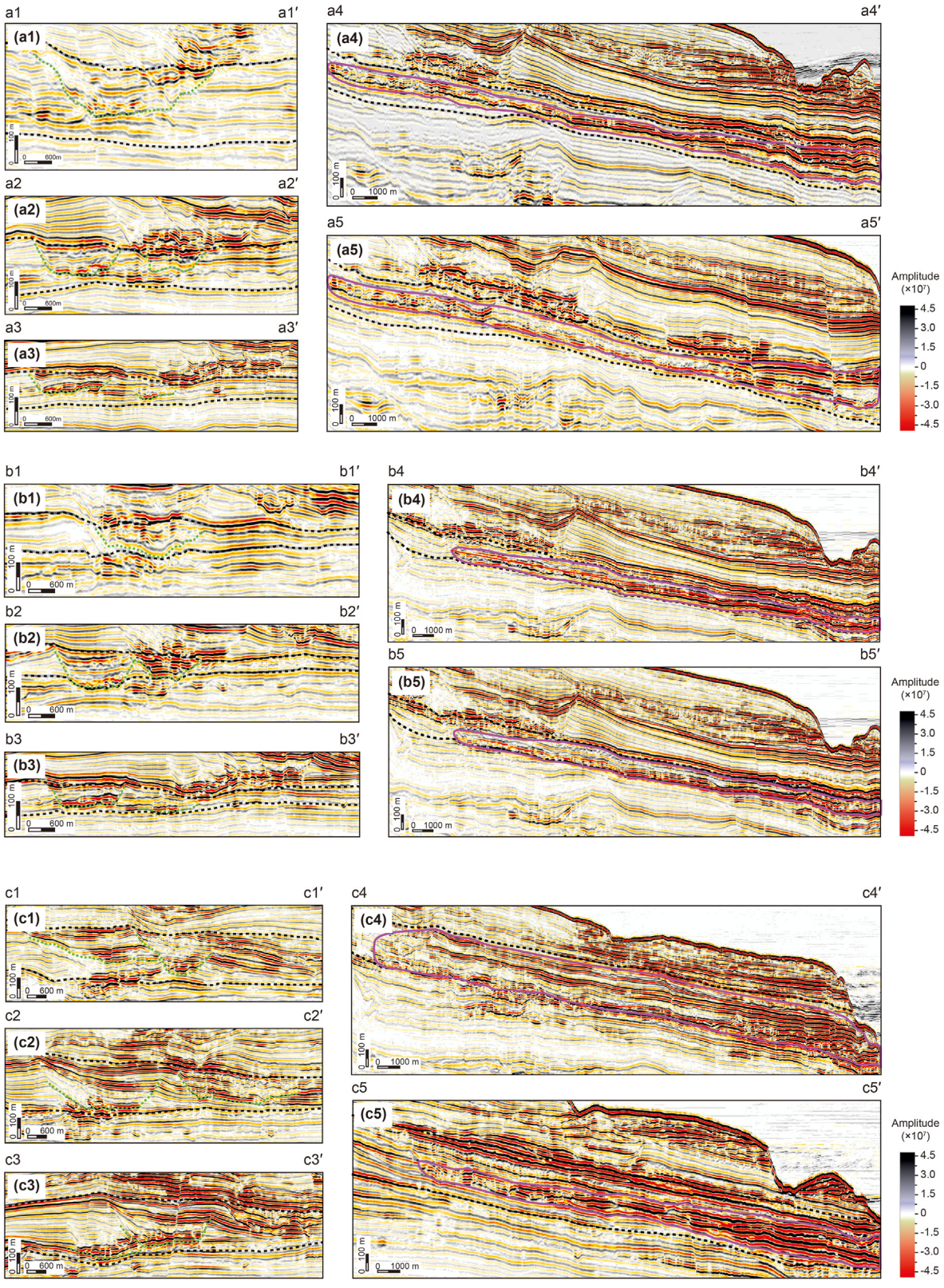

Fig. 7. Seismic amplitude maps of depositional architectural complexes A, B and C. The location of the seismic profiles is shown in Fig. 5a, b and c. The green lines indicate the boundary of the channels and the rose pink lines indicate the boundary of the lobes. The black dashed lines correspond to the seismic boundaries of the internal sequences of Pliocene-Quaternary.

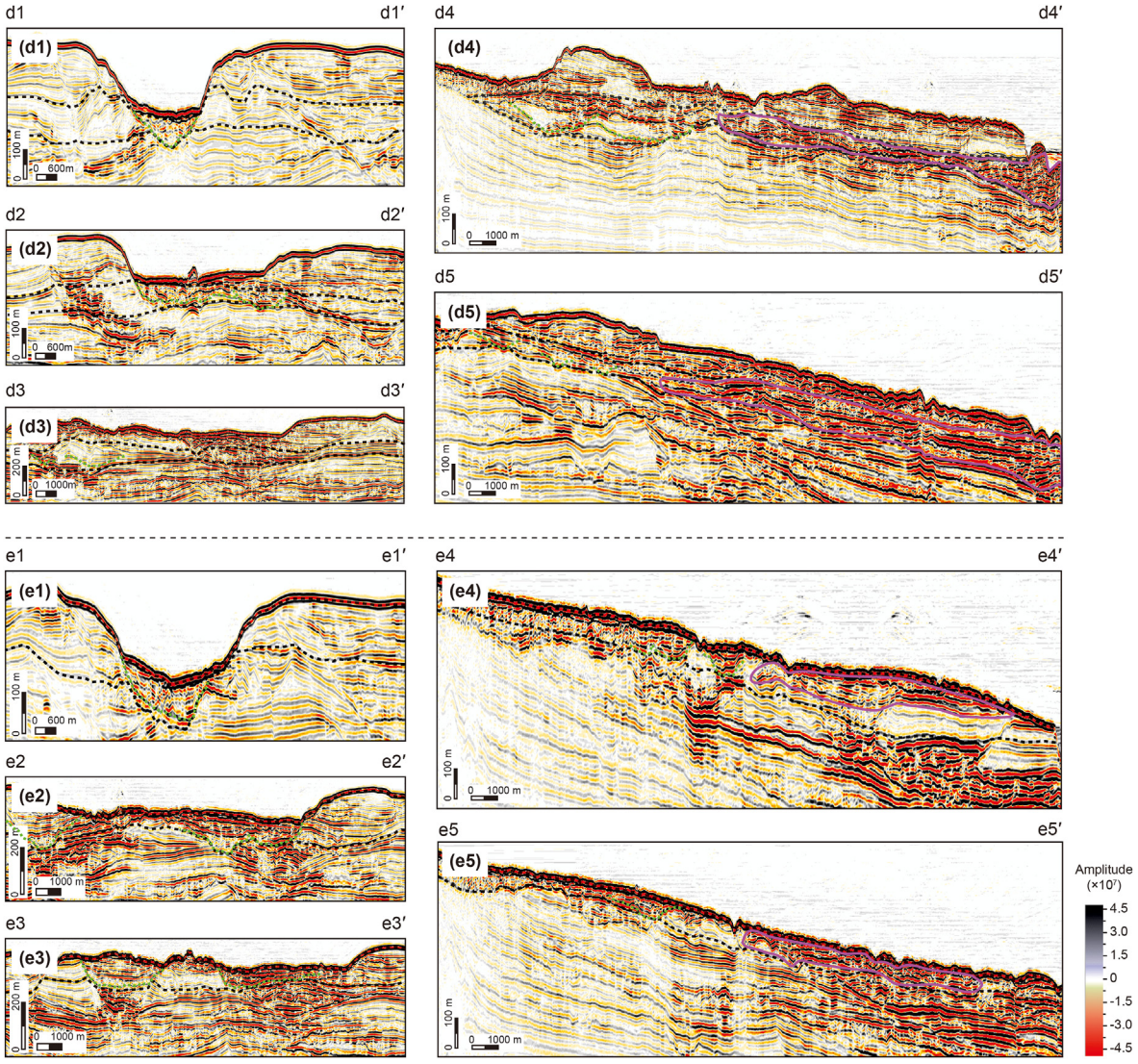

Fig. 8. Seismic amplitude maps of depositional architectural complexes D and E. The location of the seismic profiles is shown in Fig. 5d and e. The green lines indicate the boundary of the channels and the rose pink lines indicate the boundary of the lobes. The black dashed lines correspond to the seismic boundaries of the internal sequences of Pliocene-Quaternary.

Table 2
The parameters of different hierarchical channels, including length, width, length/width, average of length and width and maximum thickness.

Channel complex	Single channel	Length, m	Average length of channel complex, m	Width. m	Average width of channel complex, m	Length/ width	Average of length and width, m	Maximum thickness of channel complex, m	Maximum thickness of single channel, m
A	A1	17306	16647	1136	1152	15.23	9221.0	107	64
	A2	15985		1168		13.69	8576.5		100
B	B1	14581	14086	1646	1600	8.86	8113.5	133	130
	B2	13590		1554		8.75	7572.0		93
C	C1	12134	12250	2321	2057	5.23	7227.5	179	163
	C2	12366		1793		6.90	7079.5		148
D	D1	17862	15117	1272	1989	14.04	9567.0	116	107
	D2	12372		2705		4.57	7538.5		100
E	E1	15223	15476	1805	1677	8.43	8514.0	136	95
	E2	15728		1549		10.15	8638.5		74

Length is the maximum value of channel in the plan view.

4.3.2. Lateral slope

Fig. 10 shows the elvation depth maps (a), dip maps (b) and amplitude (c) maps of lobes. For each lobe complexes, in the upstream part of the lobe (proximal parts of units, feeder channel location), slope dip degree is lager. Inside a lobe complex, there is a difference of elvation depth and dip degree in two single lobes. For

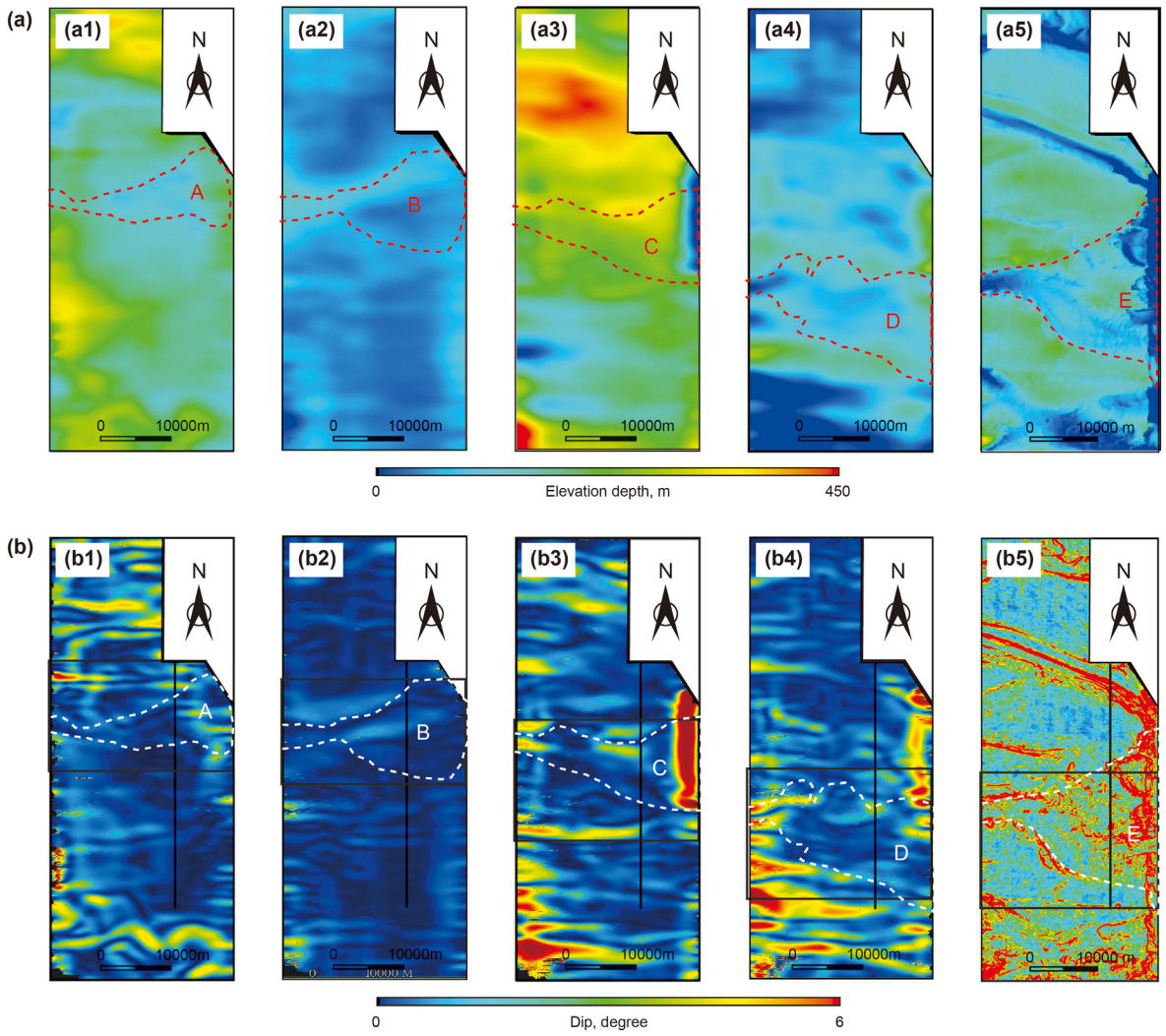

Fig. 9. Maps showing the topography (a) and the slope dip (b) before the current lobe complex was deposited (A, B, C, D and E, dashed lines).

Table 3
Longitudinal slope parameters of different hierarchical lobes, including longitudinal slope, difference in slope between single lobes within a lobe complex and average longitudinal slope within a lobe complex.

Lobe complex	Single lobe	longitudinal slope, °	Difference in slope between single lobes within a lobe complex, °	Average longitudinal slope within a lobe complex, °
A	A1	1.04	0.48	0.80
	A2	0.56		
B	B1	1.06	0.66	0.73
	B2	0.40		
C	C1	1.73	1.13	1.17
	C2	0.60		
D	D1	1.18	0.81	0.78
	D2	0.37		
E	E1	4.33	0.15	4.26
	E2	4.18		

example, elvation depth of single lobe B1 is small, but its dip is large.

Table 4 counts the specific parameters of the lateral slope. Lateral slope ranges from 0.23° to 6.42°. The maximum average lateral slope is 5.32° (lobe complex E), and the minimum is 0.41° (lobe complex E). The difference in lateral slope between two lobes ranges from 0.02° to 2.20°. The width of overlap zone ranges from 1857 m to 3720 m.

5. Discussion

5.1. Evolution of lobe architecture

Sediment transport in the Rovuma Basin generally occurs from west to east due to the topography (orientation of the general slope dip direction) (Fig. 10b). Southwards migration of different lobes (Fig. 6) is attributed due to compensational stacking (Straub and Pyles, 2012). In the following sections, we will focus on the

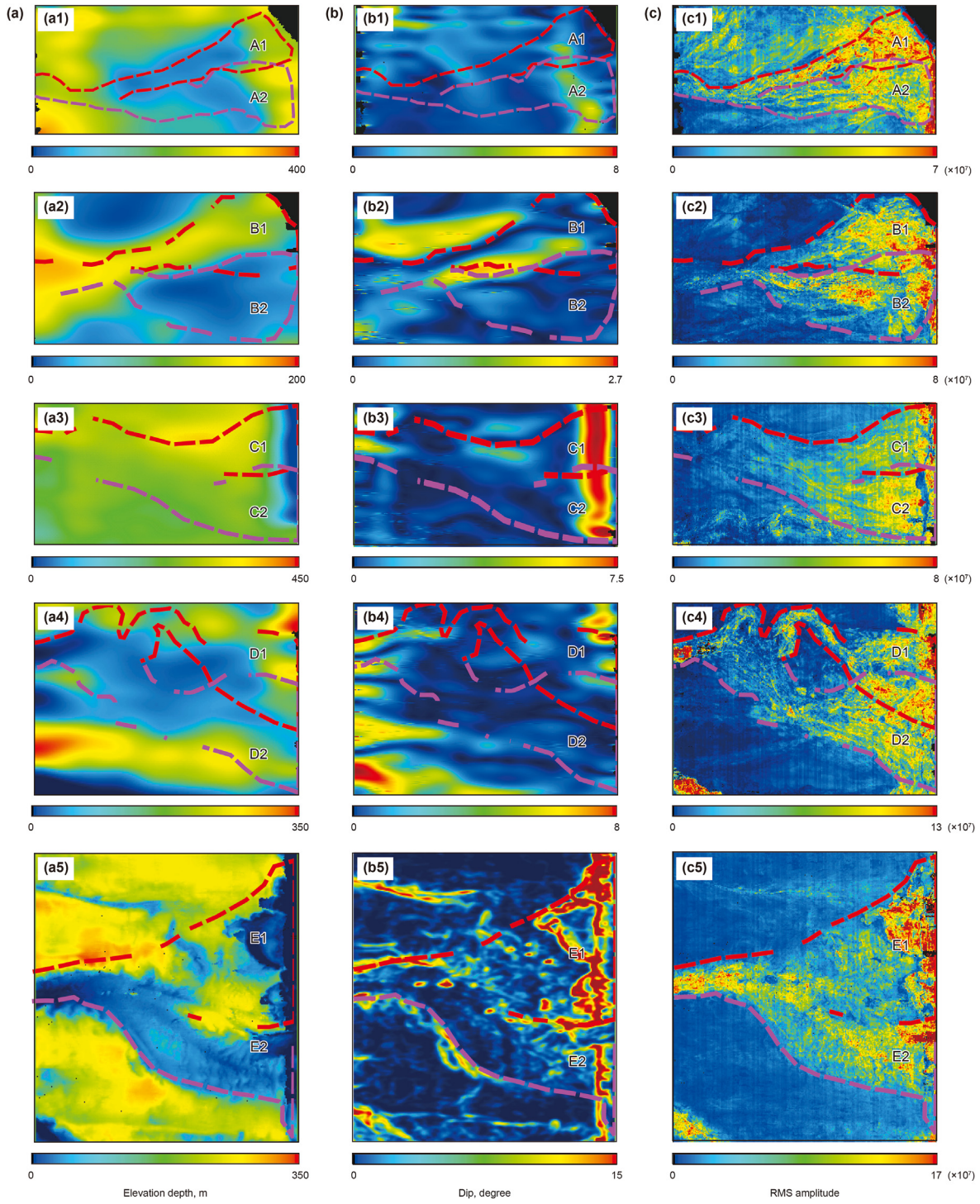

Fig. 10. Maps showing the topography (a) and the slope dip (b) before the current single lobe was deposited (A1 and A2, B1 and B2, C1 and C2, D1 and D2, E1 and E2). (c) RMS amplitude maps of Pliocene-Quaternary deposits (A1 and A2, B1 and B2, C1 and C2, D1 and D2, E1 and E2). The boundary lines (red and rose pink dashed lines) are determined by Fig. 10(c).

longitudinal and lateral growth characteristics of lobes.

5.1.1. Longitudinal growth

Submarine lobes take shape in regions where turbidity currents emerge from the confines of channels, resulting in a reduction of their ability to carry the entirety or portions of their sediment load. This phenomenon is most notably observed at the mouth of channels, where the difference in elevation between the levees is relatively modest (Adeogba et al., 2005; Deptuck and Sylvester, 2018). The longitudinal growth of lobes appears to be strongly connected to their feeder channels, which evolve from a main channel into distributary channels and eventually form single lobes (Figs. 7 and 8).

Table 4
Lateral slope parameters of different hierarchical lobes, including lateral slope, difference in slope between single lobes within a lobe complex and average longitudinal slope within a lobe complex.

Lobe complex	Single lobe	Lateral slope, °	Averages of lateral slope within a lobe complex, °	Difference of lateral slope between two single lobes within a lobe complex, °	Overlap width, m
A	A1	1.25	1.435	0.37	1857
	A2	1.62			
B	B1	0.59	0.41	0.36	2158
	B2	0.23			
C	C1	0.97	0.755	0.43	3720
	C2	0.54			
D	D1	0.99	0.98	0.02	2728
	D2	0.97			
E	E1	6.42	5.32	2.20	2952
	E2	4.22			

5.1.2. Lateral growth

Lobe migration characterizes the lateral organization of the architectural elements on lobes. In the Pliocene-Quaternary strata of the Rovuma Basin, the identified lobes primarily consist of two hierarchical types: single lobes and lobe complexes. Overall, channel-lobe complexes showed southward migration, as the low topography gradually moves southward. Single lobes in all lobe complexes are also preferentially deposited in the lower north. Their lateral evolution will be here discussed separately.

1) The lateral evolution of single lobes in the Rovuma Basin can be characterized by two stages. As the terrain in the central area is low, the first single lobe is initially deposited in the north central area (Figs. 6 and 9a). After the first single lobe is deposited in the north, the subsequent single lobe is deposited in lower terrain to the south. Firstly, lobe A1 is deposited, followed by lobe A2 south of A1. This results in the southwards migration of single lobes B1 and B2, C1 and C2, D1 and D2, E1 and E2, which are stacked one after the other, resulting in a unidirectional northward migration.
2) The lateral evolution of lobe complexes follows a clear migration trend. In the upstream portion of the lobe complexes (proximal parts of units), deposition typically occurs in topographic lows. The architecture complex A (Fig. 9) is first deposited in the lowest part of the northern terrain (Fig. 11a). After the lobe complex A is deposited, the lower part migrates southward, leading to the deposition of the lobe complex B in the southern part of the lobe complex A (Fig. 11b). Subsequently, the lobe complex C is deposited in the southern part of the lobe complex B (Fig. 11c). This pattern is repeated by the lobe complexes D and E (Fig. 11c, d and e). As a result, the stacking pattern of lobe complexes demonstrates a southward migration (Fig. 11e).

5.2. Effects of previous topography on lobe architecture

The geometry of submarine lobes is known to be influenced by the seafloor topography (Gervais et al., 2006; Saller et al., 2008; Prélat et al., 2010; Spychala et al., 2017, 2020). The location where the lobe deposits form is determined by the shape of the seafloor created by previous deposits (as discussed in Section 5.1). With this in mind, we conducted a detailed investigation into the effects of longitudinal and lateral slopes on the shape, size, and growth patterns of lobes. The deposition position and migration sequence of the lobe complex are mainly related to topography. Considering a relatively constant sediment supply, we assume that the sediment supply of single lobes was similar and then compare the control of slope as an individual factor for single lobes.

5.2.1. Effects of longitudinal slope on lobe architecture

Single lobes are deposited first at positions with a steeper longitudinal slope gradient (Table 3). Compared with the lobe E with a larger slope, the lobes A, B, C, and D with a gentle slope are generally smaller in length and larger in width (Tables 1 and 3). As the longitudinal slope gradient increases, the aspect ratio of the lobes seems increases. As a result, single lobes tend to be more rounded in shape when the longitudinal slope gradient is low and more elongated when the slope gradient is high (Fig. 13a).

5.2.2. Effects of lateral slope on lobe architecture

When the lateral slope is steep, they tend to overlap more extensively, particularly when deposited on a low slope gradient (R^2 = 0.99, Figs. 12a and 13b). Our results also show that as the average of the lateral and longitudinal slope gradients increases, the width-to-thickness ratio of the lobe decreases, meaning that sediments tend to accumulate more vertically (Figs. 12b and 13c).

To summarize, our study reveals that the effects of the slope system on the location and dimensions of the deposits are multifaceted: a) a steeper longitudinal slope results in more slender lobes (Fig. 13a); b) a steeper lateral slope results in a larger overlap width between lobes (Fig. 13b); and c) an increase in both lateral and longitudinal slope gradients prompts sediments to accumulate in a more vertically oriented manner (Fig. 13c).

5.3. Comparison with other lobe deposits and analogue experiments affected by topography

The study of submarine lobe architecture provides valuable insights into the paleogeographic setting and the extent of basin confinement (Spychala et al., 2015, 2017; Ferguson et al., 2020). This study, along with previous works, highlights that the architecture of submarine lobes is significantly influenced by pre-existing topography (Lee et al., 1999; Gervais et al., 2006; Prélat et al., 2010; Gamboa and Alves, 2015; Koo et al., 2016; Picot et al., 2016; Spychala et al., 2017, 2020; Brooks et al., 2018; Kuswandaru et al., 2019; Zhang and Wu, 2019; Fryer et al., 2021; Silva et al., 2020). This effect can be observed in modern and ancient deposits, as well as in physical (flume-tank experiments) experiments and numerical simulations. We tried to compare our measurements with those in other lobe deposits and experiments.

5.3.1. Comparison with other lobe deposits

Previous studies have indicated that the internal architecture of lobe deposits is controlled by the confinement of gravity current and antecedent topography (Lee et al., 1999). It has been found that lateral slope confinement on one side promotes lateral migrations of lobes (Gervais et al., 2006). As the degree of lateral confinement on both sides increases, the lateral width of lobe complexes

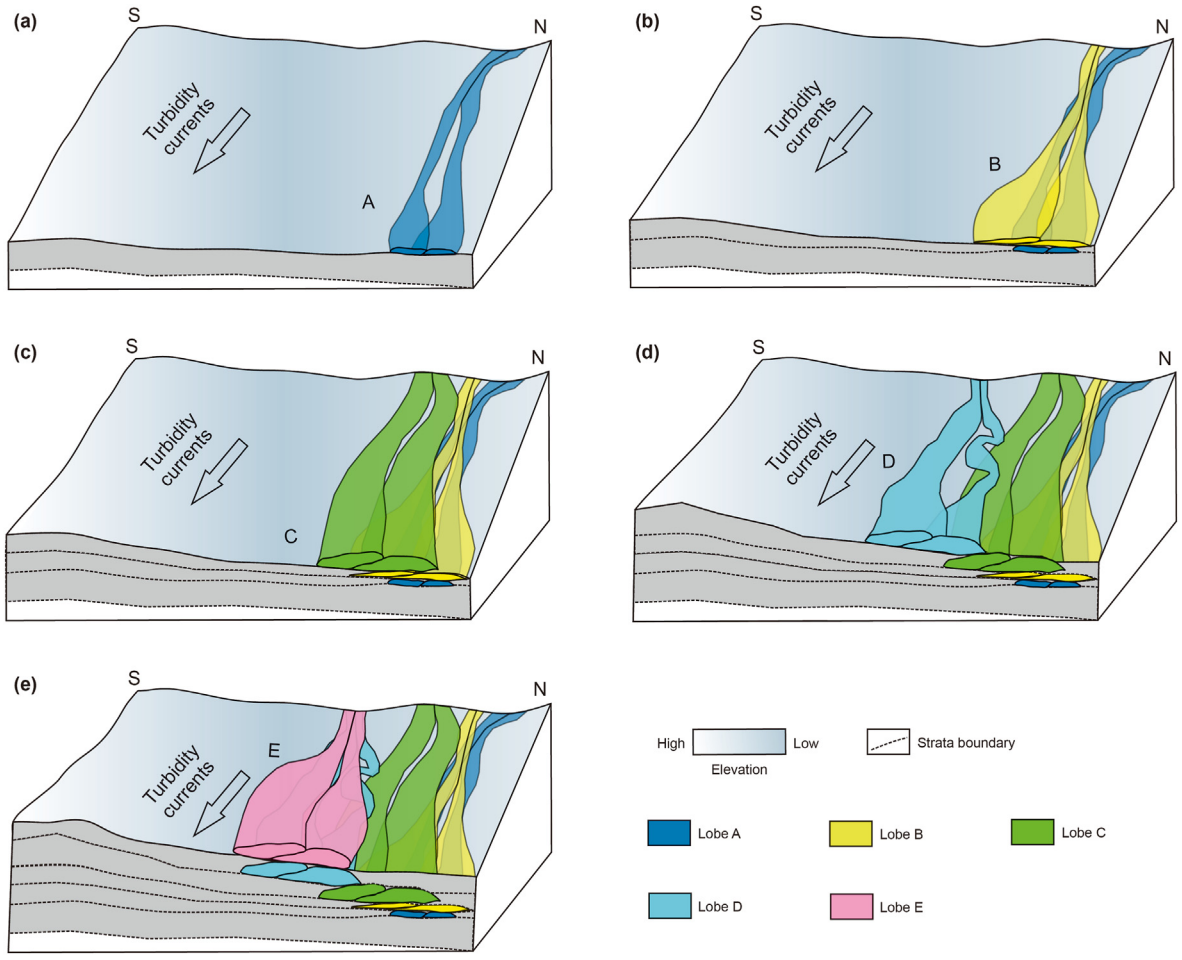

Fig. 11. Schematic diagram of the depositional process of lobe complexes and single lobes. Lobe complexes are displayed in different colors. Single lobes are separated by solid black lines in the same color. (a) Depicts the initial stage of channel-lobe deposition, specifically lobe A in Sq1, where the terrain exhibits a low elevation. (b) Following the deposition of channel-lobe A, the second stage showcases channel-lobe deposition B, which is laid down in Sq2 and overlies the previously deposited channel-lobe A system. (c) Represents the occurrence of channel-lobe deposition C in Sq3 after channel-lobe B deposition. Notably, this deposition location has shifted southward. (d) Depicts the emergence of channel-lobe deposition D in Sq4 after channel-lobe C deposition. The southward migration distance increases as the low topography location shifts further south. (e) Concludes with lobe deposition E in Sq5, occurring after channel-lobe D deposition and overlaying the D system. In all channel-lobe complexes, single lobes were preferentially deposited at lower northern locations.

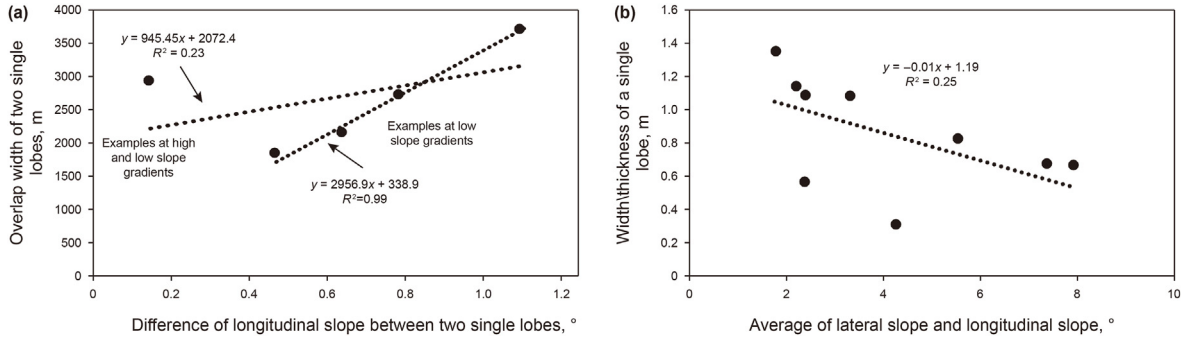

Fig. 12. (a) Overlap width of two single lobes vs. difference of longitudinal slope between two single lobes. Left regression line is derived from samples taken across all lobe complexes including high and low slope gradients. Right regression line is constructed based on samples collected exclusively from lobe complexes A, B, C, and D which are at low slope gradients. (b) Width/thickness of single lobes vs. average of lateral slope and longitudinal slopes.

decrease and the longitudinal length of lobe complexes increase (Zhang and Wu, 2019). The effects of longitudinal slope on lobe architecture can be attributed to both the continental slope (the location of feeder channel deposits) and the basin slope (the location of lobe deposits).

In our study, we quantitatively investigated the effect of lateral slope on lobe architecture, revealing the control of lateral slope itself and accompanied with longitudinal slope on lobe morphology and stacking pattern. Our findings go beyond the qualitative study of the degree of lateral confinement of the terrain.

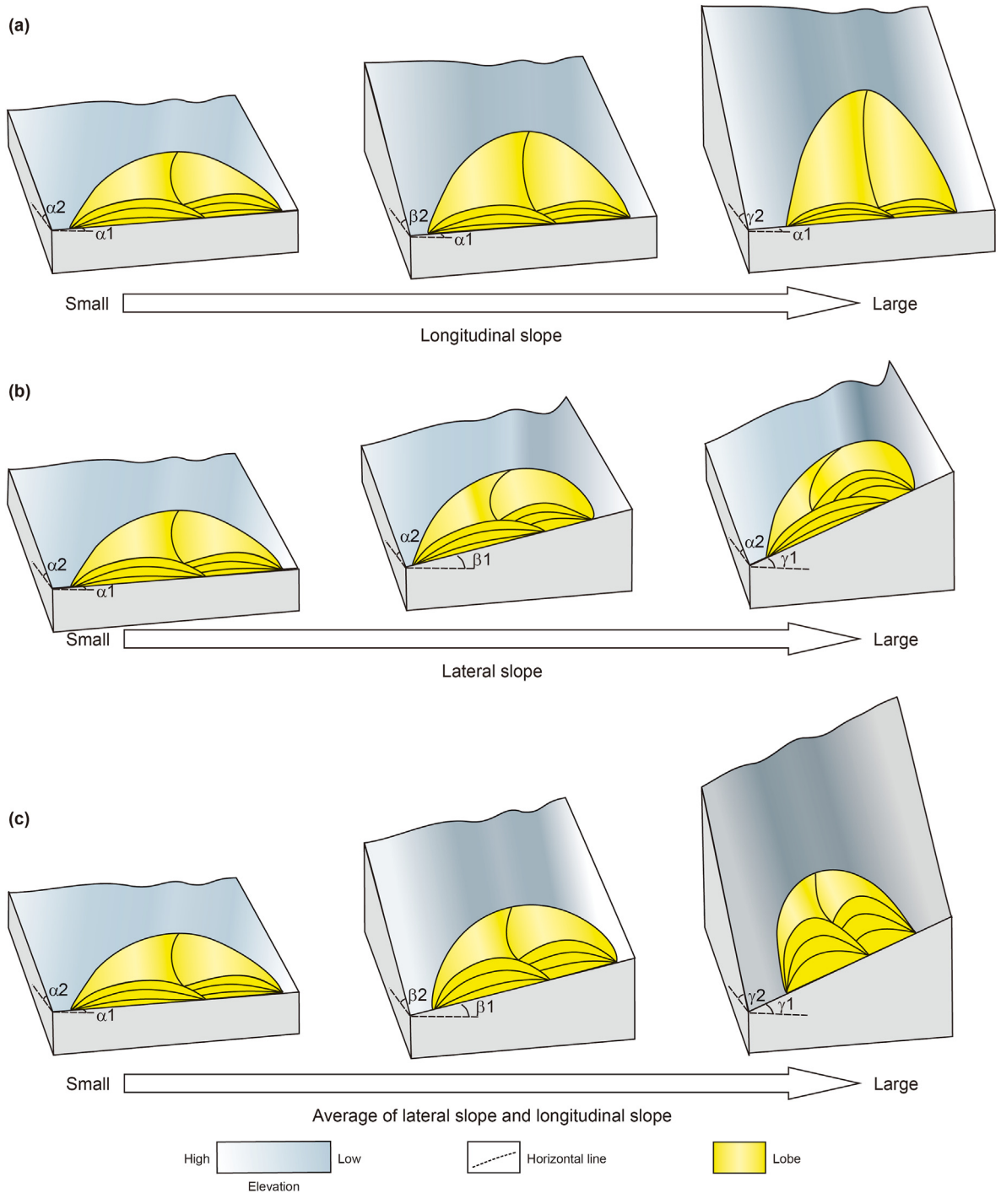

Fig. 13. Lobe stacking pattern vs. slope. (a) Aspect ratio of lobes increases with increasing longitudinal length. (b) Overlap width between lobes increases with increasing lateral length. (c) Thickness of lobe increases with increasing average of lateral slope and longitudinal slope.

Furthermore, we found a stronger connection between the longitudinal growth of lobes and their feeder channels.

5.3.2. Comparison with analogue experiments

Previous studies using analogue experiments provide valuable insights into the effects of slope on lobe architecture (i.e. flume-tank experiments, Steel et al., 2017; Spychala et al., 2020). They can help to understand the complex relationships between slope and lobe architecture, as well as test different hypotheses. However, it is important to keep in mind that the results obtained from analogue experiments may not perfectly match the real-world scenarios, due to differences in the scale, boundary conditions, and other factors. Therefore, it is necessary to consider the limitations and uncertainties of these experiments when interpreting the

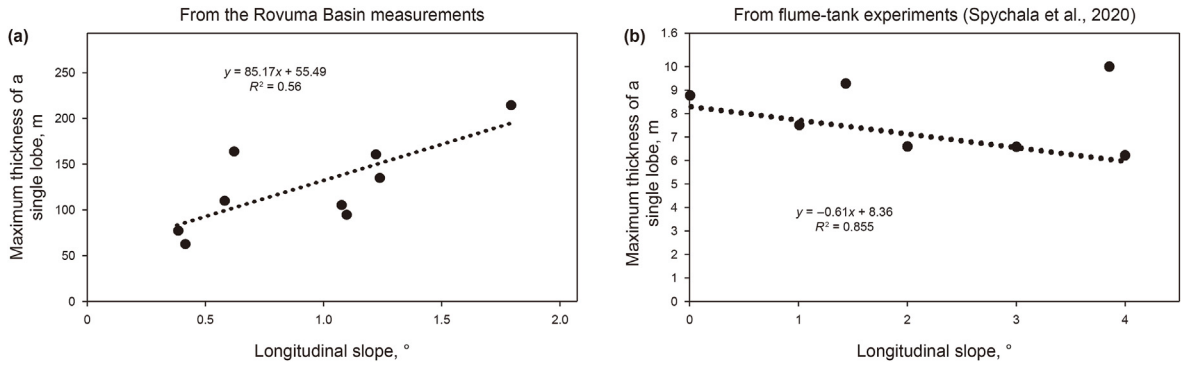

Fig. 14. Maximum thickness of a single lobe vs. longitudinal slope. (a) is from the Rovuma Basin measurements and (b) is from flume-tank experiments (based on Spychala et al., 2020).

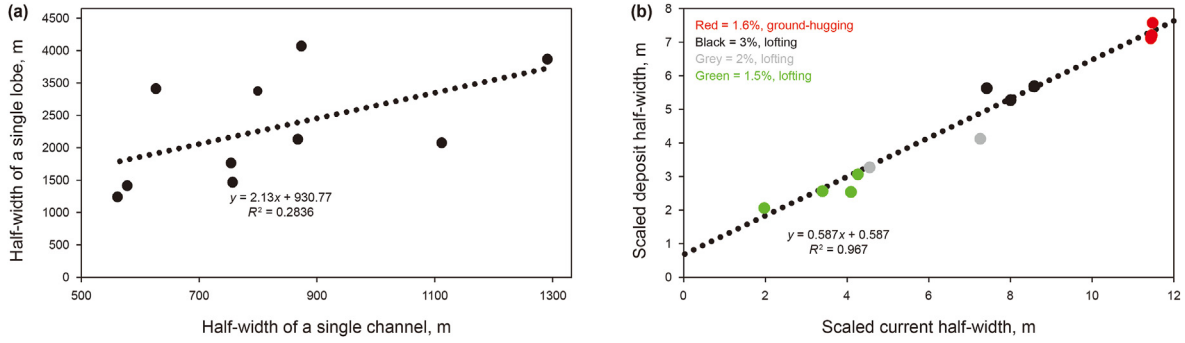

Fig. 15. (a) Half-width of a single lobe vs. half-width of a single channel in the Rovuma Basin and (b) scaled current half-width vs. scaled deposit half-width, which is from flume-tank experiments (edited from Steel et al., 2017).

results. We compared the difference between the deposition data in nature system and the experimental data and analyzed the possible reasons.

5.3.2.1. Relationship between longitudinal slope and thickness of lobes. We found that maximum thickness increases as the longitudinal slope increases (Fig. 14a). In comparison with the previous quantitative physical simulation experiment on the effect of longitudinal slope on lobe architectures (Spychala et al., 2020), their studies found that as longitudinal slope increases, the maximum thickness decreases (Fig. 14b). This suggests that the maximum thickness of lobe is not only affected by the radial slope, but also controlled by other factors. In this study, the restriction of the lateral slope also plays a role in the lobe architecture (Fig. 13c). An increase in both lateral and longitudinal slope gradients prompts sediments to accumulate more vertically and develop larger thickness. This suggests that the various parameters of the terrain should be comprehensively considered to understand the controlling factors and their effect on the lobe architecture.

5.3.2.2. Relationship between lobe width and channel width. The size of feeder channel determines the total amount of fed sediment (Hodgson et al., 2016), and the total amount of fed sediment also determines the size of the lobe. In our study, the half-width (half of the maximum lateral width of the lobe) of lobe deposition is also positively correlated with the half-width of the feeder channel (Fig. 15a). In physical simulation experiment on the effect of feeder current size on fan deposits geometry of Steel et al. (2017), it is found that there is a strong linear relationship between current half-width and deposit half-width. This suggests that factors that influence the lateral spreading of currents will similarly impact deposits geometry (Fig. 15b). The width of feeder channel can approximately indicate the width of the currents in Fig. 15. Their differences in correlation coefficients may reflect differences in sediment concentration and grain size between natural and experimental system. Our depositional environment measurements offer more data and possibility for quantitative correlation studies.

Our work offers a systematic study on how the shape of slopes influences the 3-D architecture of seafloor lobes in natural deep-sea systems. The results of our quantitative analysis can be used as a reference for predicting lobe architecture in similar topographical cases in other regions. This is significant for predicting the boundary of subsurface deposits. Additionally, the migration of lobes can also be influenced by other factors, such as sediment supply and basin configuration. Due to same depositional environment, different lobe deposits in our study area can be considered to have similar sediment concentration and sediment grain size. The correlation between precedent topography and lobe migration provides crucial insights into the sedimentary processes that shape the subsurface architecture in the Rovuma Basin. Overall, this study highlights the importance of incorporating topographic analysis in the interpretation of subsurface sedimentary systems.

The current study specifically investigates the influence of longitudinal slope and lateral slope on both lobe complexes and individual lobe architecture. This research contributes to our comprehension of the shape, size, and stacking patterns within a channel-lobe system situated in a slope environment. This insight builds upon earlier findings that acknowledged topographical control over the broader submarine fan system (Gervais et al., 2006; Zhang and Wu, 2019; Spychala et al., 2020).

Explorations into submarine fan architecture can be harnessed to analyze impediments and heterogeneities in fluid flow within reservoirs, thereby offering pragmatic guidance for reservoir development (Prélat et al., 2009, 2010; Prélat and Hodgson, 2013; Yu et al., 2014; Zhang et al., 2016; Zhang et al., 2018). By providing a meticulous characterization of lobe architecture within a specific system, our investigations offer a blueprint for examining depositional patterns in analogous scenarios.

6. Conclusions

In this study, we analyze the effects of topography factors (longitudinal slope and lateral slope) on lobe complex and single lobe architecture (shape, size and growth pattern). The results indicate that topography determines preferential deposition of lobe complexes and single lobes.

When the topography is irregular and presents topographic lows, lobe complexes first infill these depressions. Single lobes are deposited preferentially at positions with higher longitudinal slope gradients. As the longitudinal slope becomes higher, the aspect ratio of the single lobes increases. Lateral topography does not seem to have a strong influence on the shape of single lobe, but it seems to affect the overlap of single lobes. When the lateral slope gradient is relatively high, the single lobes tend to have a larger overlap surface. Furthermore, as the average of lateral slope and longitudinal slope gets greater, the width/thickness of single lobe is smaller, i.e. sediments tend to accumulate vertically.

Declaration of competing interest

We declare that we do not have any commercial or associative interest that represents a conflict of interest in connection with the work submitted.

Acknowledgements

The study is funded by the Cooperation Project of China National Petroleum Company (CNPC) and China University of Petroleum-Beijing (CUPB) (No. RIPED-2021-JS-552), the National Natural Science Foundation of China (Nos.42002112,42272110), the Strategic Cooperation Technology Projects of CNPC and CUPB (No. ZLZX2020-02) and the Science Foundation for Youth Scholars of CUPB (No. 24620222BJRC006). We thank the China Scholarship Council (CSC) (No. 202106440048) for having funded the research stay of Mei Chen at MARUM, University of Bremen. We thank Elda Miramontes for her constructive comments and suggestions that helped us improve our manuscript.

References

Adeogba, A.A., McHargue, T.R., Graham, S.A., 2005. Transient fan architecture and depositional controls from near-surface 3-D seismic data, Niger Delta continental slope. AAPG Bulletin 89 (5), 627–643. https://doi.org/10.1306/11200404025.

Breitzke, M., Wiles, E., Krocker, R., et al., 2017. Seafloor morphology in the Mozambique Channel: evidence for long-term persistent bottom-current flow and deep-reaching eddy activity. Marine Geophysical Research 38, 241–269. https://doi.org/10.1007/s11001-017-9322-7.

Brooks, H.L., Hodgson, D.M., Brunt, R.L., Peakall, J., Poyatos-Moré, M., Flint, S.S., 2018. Disconnected submarine lobes as a record of stepped slope evolution over multiple sea-level cycles. Geosphere 14 (4), 1753–1779. https://doi.org/10.1130/GES01618.1.

Cao, Q., Tang, P., Lü, F., 2018. Formation conditions and controlling factors of gas-bearing turbidite sand reservoirs in deep water deposits in the Rovuma Basin, East Africa. Marine Origin Petroleum Geology 23 (3), 65–72. https://doi.org/10.3969/j.issn.1672-9854.2018.03.007.

Chen, M., Wu, S., Wang, R., et al., 2023. Sedimentary architecture of submarine lobes affected by bottom currents: Insights from the Rovuma Basin offshore East Africa. Basin Research. https://doi.org/10.1111/bre.12829.

Chen, Y., Yao, G., Lu, Y., Chen, L., Tang, P., Cao, Q., 2017. Sedimentary characteristics and controlling factors of Oligocene deep-water channel-lobe in Rovuma Basin of the East Africa. Acta Petrolei Sinica 38 (9), 1047. https://doi.org/10.7623/syxb201709006.

Chen, Y.H., Yao, G.S., Lü, F.L., Tang, P., Lu, Y., 2016. Tectonic-sedimentary evolution and petroleum geology characteristics in deepwater area in Rovuma basin, East Africa. Mar. Origin Petrol. Geol. 21 (2), 39–46. https://doi.org/10.3969/j.issn.1672-9854.2016.02.005.

Collins, C., Hermes, J.C., Roman, R.E., Reason, C.J.C., 2016. First dedicated hydrographic survey of the Comoros Basin. J. Geophys. Res. Oceans 121 (2), 1291–1305. https://doi.org/10.1002/2015JC011418.

Deptuck, M.E., Sylvester, Z., 2018. Submarine fans and their channels, levees, and lobes. In: Submarine Geomorphology. Springer, Cham, pp. 273–299. https://doi.org/10.1007/978-3-319-57852-1_15.

Deptuck, M.E., Piper, D.J., Savoye, B., Gervais, A., 2008. Dimensions and architecture of late Pleistocene submarine lobes off the northern margin of East Corsica. Sedimentology 55 (4), 869–898. https://doi.org/10.1111/j.1365-3091.2007.00926.x.

Ferguson, R.A., Kane, I.A., Eggenhuisen, J.T., Pohl, F., Tilston, M., Spychala, Y.T., Brunt, R.L., 2020. Entangled external and internal controls on submarine fan evolution: an experimental perspective. The Depositional Record 6 (3), 605–624. https://doi.org/10.1002/dep2.109.

Fonnesu, M., Palermo, D., Galbiati, M., Marchesini, M., Bonamini, E., Bendias, D., 2020. A new world-class deep-water play-type, deposited by the syndepositional interaction of turbidity flows and bottom currents: the giant Eocene Coral Field in northern Mozambique. Mar. Petrol. Geol. 111, 179–201. https://doi.org/10.1016/j.marpetgeo.2019.07.047.

Fryer, R.C., Jobe, Z.R., Laugier, F., Pettinga, L.A., Gilbert, J.C., Shumaker, L.E., Smith IV, J.E., Sullivan, M., 2021. Submarine lobe deposits of the Point Loma Formation, California: quantifying event-bed architecture and lateral heterogeneity. The Depositional Record 7 (3), 374–391. https://doi.org/10.1002/dep2.156.

Fuhrmann, A., Kane, I.A., Clare, M.A., Ferguson, R.A., Schomacker, E., Bonamini, E., Contreras, F.A., 2020. Hybrid turbidite-drift channel complexes: an integrated multiscale model. Geology 48 (6), 562–568. https://doi.org/10.1130/G47179.1.

Gamboa, D., Alves, T.M., 2015. Spatial and dimensional relationships of submarine slope architectural elements: a seismic-scale analysis from the Espírito Santo Basin (SE Brazil). Mar. Petrol. Geol. 64, 43–57. https://doi.org/10.1016/j.marpetgeo.2015.02.035.

Gervais, A., Savoye, B., Mulder, T., Gonthier, E., 2006. Sandy modern turbidite lobes: a new insight from high resolution seismic data. Mar. Petrol. Geol. 23 (4), 485–502. https://doi.org/10.1016/j.marpetgeo.2005.10.006.

Hodgson, D.M., Kane, I.A., Flint, S.S., Brunt, R.L., Ortiz-Karpf, A., 2016. Time-transgressive confinement on the slope and the progradation of basin-floor fans: implications for the sequence stratigraphy of deep-water deposits. J. Sediment. Res. 86 (1), 73–86. https://doi.org/10.2110/jsr.2016.3.

Koo, W.M., Olariu, C., Steel, R.J., Olariu, M.I., Carvajal, C.R., Kim, W., 2016. Coupling between shelf-edge architecture and submarine-fan growth style in a supply-dominated margin. J. Sediment. Res. 86 (6), 613–628. https://doi.org/10.2110/jsr.2016.42.

Kus, K.B., Jobe, Z.R., Laugier, F., Walker, W., Sullivan, M., 2022. Quantifying the lateral heterogeneity of distal submarine lobe deposits, Point Loma Formation, California: implications for subsurface lateral facies prediction. The Depositional Record 8 (2), 472–501. https://doi.org/10.1002/dep2.169.

Kuswandaru, G.Y., Amir Hassan, M.H., Matenco, L.C., Taib, N.I., Mustapha, K.A., 2019. Turbidite, debrite, and hybrid event beds in submarine lobe deposits of the Palaeocene to middle Eocene Kapit and Pelagus members, Belaga Formation, Sarawak, Malaysia. Geol. J. 54 (6), 3421–3437. https://doi.org/10.1002/gj.3347.

Lee, S.H., Chough, S.K., Back, G.G., Kim, Y.B., Sung, B.S., 1999. Gradual downslope change in high-resolution acoustic characters and geometry of large-scale submarine debris lobes in Ulleung Basin, East Sea (Sea of Japan), Korea. Geo Mar. Lett. 19 (4), 254–261. https://doi.org/10.1007/s003670050116.

Liu, Z.Y., Lü, M., Lu, J.M., Lü, D., Wang, Y., Guo, G., 2017. Deepwater depositional system in the background of narrow shelf in the ruvuma basin, eastern Africa. Mar. Origin Petrol. Geol. 22 (4), 27–34. doi:10.3969/j.issn.1672-9854.2017.04.004.(in Chinese).

Lowe, D.R., 1982. Sediment gravity flows; II, Depositional models with special reference to the deposits of high-density turbidity currents. J. Sediment. Res. 52 (1), 279–297. https://doi.org/10.1306/212F7F31-2B24-11D7-8648000102C1865D.

Luan, X., Lu, Y., Fan, G., Ran, W., 2021. Deep-water sedimentation controlled by interaction between bottom current and gravity flow: a case study of Rovuma Basin, East Africa. J. Afr. Earth Sci. 180, 104228. https://doi.org/10.1016/j.jafrearsci.2021.104228.

Miramontes, E., Thiéblemont, A., Babonneau, N., et al., 2021. Contourite and mixed turbidite-contourite systems in the Mozambique Channel (SW Indian Ocean): link between geometry, sediment characteristics and modelled bottom currents. Marine Geology 437, 106502. https://doi.org/10.1016/j.margeo.2021.106502.

Mulder, T., Etienne, S., 2010. Lobes in deep-sea turbidite systems: state of the art. Sediment. Geol. 3 (229), 75–80. https://doi.org/10.1016/2Fj.sedgeo.2010.06.011.

Mutti, E., 1977. Distinctive thin-bedded turbidite facies and related depositional environments in the Eocene Hecho Group (South-central Pyrenees, Spain). Sedimentology 24 (1), 107–131. https://doi.org/10.1111/j.1365-3091.1977.tb00122.x.

Mutti, E., Normark, W.R., 1987. Comparing examples of modern and ancient

turbidite systems: problems and concepts. In: Marine Clastic Sedimentology: Concepts and Case Studies, pp. 1–38.
Normark, W.R., 1978. Fan valleys, channels, and depositional lobes on modern submarine fans: characters for recognition of sandy turbidite environments. AAPG (Am. Assoc. Pet. Geol.) Bull. 62 (6), 912–931. https://doi.org/10.1306/C1EA4F72-16C9-11D7-8645000102C1865D.
Picot, M., Droz, L., Marsset, T., Dennielou, B., Bez, M., 2016. Controls on turbidite sedimentation: insights from a quantitative approach of submarine channel and lobe architecture (Late Quaternary Congo Fan). Mar. Petrol. Geol. 72, 423–446. https://doi.org/10.1016/j.marpetgeo.2016.02.004.
Prélat, A., Hodgson, D.M., Flint, S.S., 2009. Evolution, architecture and hierarchy of distributary deep-water deposits: a high-resolution outcrop investigation from the Permian Karoo Basin, South Africa. Sedimentology 56 (7), 2132–2154. https://doi.org/10.1111/j.1365- 3091.2009.01073.x.
Prélat, A., Covault, J.A., Hodgson, D.M., Fildani, A., Flint, S.S., 2010. Intrinsic controls on the range of volumes, morphologies, and dimensions of submarine lobes. Sediment. Geol. 232 (1–2), 66–76. https://doi.org/10.1016/j.sedgeo.2010.09.010.
Prélat, A., Hodgson, D.M., 2013. The full range of turbidite bed thickness patterns in submarine lobes: controls and implications. J. Geol. Soc. 170 (1), 209–214. https://doi.org/10.1144/jgs2012-056.
Saller, A., Werner, K., Sugiaman, F., Cebastiant, A., May, R., Glenn, D., Barker, C., 2008. Characteristics of Pleistocene deep-water fan lobes and their application to an upper Miocene reservoir model, offshore East Kalimantan, Indonesia. AAPG (Am. Assoc. Pet. Geol.) Bull. 92 (7), 919–949. https://doi.org/10.1306/03310807110.
Shanmugam, G., 2016. Submarine fans: a critical retrospective 1950–2015. J. Palaeogeogr. 5 (2), 110–184. https://doi.org/10.1016/j.jop.2015.08.011.
Silva, D.B.D., Cronin, B., Celik, H., Goldberg, K., Kneller, B.C., Gürbüz, K., 2020. Evolution of two overlapping sand-rich clastic submarine fans in the Lower Miocene Adana Basin, southern Turkey: contribution from a new palaeocurrent analysis. Turk. J. Earth Sci. 29 (5), 764–784. https://doi.org/10.3906/yer-1912-14.
Spychala, Y.T., Eggenhuisen, J.T., Tilston, M., Pohl, F., 2020. The influence of basin setting and turbidity current properties on the dimensions of submarine lobe elements. Sedimentology 67 (7), 3471–3491. https://doi.org/10.1111/sed.12751.
Spychala, Y.T., Hodgson, D.M., Flint, S.S., Mountney, N.P., 2015. Constraining the sedimentology and stratigraphy of submarine intraslope lobe deposits using exhumed examples from the Karoo Basin, South Africa. Sediment. Geol. 322, 67–81. https://doi.org/10.1016/j.sedgeo.2015.03.013.
Spychala, Y.T., Hodgson, D.M., Prélat, A., Kane, I.A., Flint, S.S., Mountney, N.P., 2017. Frontal and lateral submarine lobe fringes: comparing sedimentary facies, architecture and flow processes. J. Sediment. Res. 87 (1), 75–96. https://doi.org/10.2110/jsr.2017.2.
Steel, E., Buttles, J., Simms, A.R., Mohrig, D., Meiburg, E., 2017. The role of buoyancy reversal in turbidite deposition and submarine fan geometry. Geology 45 (1), 35–38. https://doi.org/10.1130/G38446.1.
Straub, K.M., Pyles, D.R., 2012. Quantifying the hierarchical organization of compensation in submarine fans using surface statistics. J. Sediment. Res. 82 (11), 889–898. https://doi.org/10.2110/jsr.2012.73.
Vail, P.R., 1987. Seismic Stratigraphy Interpretation Using Sequence Stratigraphy: Part 1: Seismic Stratigraphy Interpretation Procedure, pp. 1–10.
Yu, L.I.N., Shenghe, W.U., Xing, W.A.N.G., Xiaoming, Z., Yun, L., Yao, L., Jiajia, Z., 2014. Research on reservoir architecture models of deep-water turbidite lobes. Nat. Gas Geosci. 25 (8), 1197–1204.
Zhang, J., Wu, S., 2019. Research progress on the depositional architecture of submarine-fan lobes. China Offshore Oil Gas 31 (5), 88–106. https://doi.org/10.11935/j.issn.1673-1506.2019.05.010.
Zhang, J., Wu, S., Hu, G., Fan, T.E., Yu, B., Lin, P., & Jiang, S., 2018. Sea-level control on the submarine fan architecture in a Deepwater sequence of The Niger Delta Basin. Mar. Petrol. Geol. 94, 179–197. doi:10.1016/j.marpe tgeo.2018.04.002.
Zhang, J.J., Wu, S.H., Fan, T.E., et al., 2016. Research on the architecture of submarine-fan lobes in The Niger Delta Basin, offshore West Africa. J. Palaeogeogr. 5 (3), 185–204. https://doi.org/10.1016/j.jop.2016.05.005.